# Frictional Magneto-Coulomb Drag in Graphene Double-Layer Heterostructures

Xiaomeng Liu,[1] Lei Wang,[2] Kin Chung Fong,[3] Yuanda Gao,[4] Patrick Maher,[5] Kenji Watanabe,[6] Takashi Taniguchi,[6] James Hone,[4] Cory Dean,[5] and Philip Kim[1,*]

[1]Department of Physics, Harvard University, Cambridge, Massachusetts 02138, USA
[2]Kevli Institute at Cornell for Nanoscale Science, Ithaca, New York 14853, USA
[3]Raytheon BBN Technologies, Quantum Information Processing Group, Cambridge, Massachusetts 02138, USA
[4]Department of Mechanical Engineering, Columbia University, New York, New York 10027, USA
[5]Department of Physics, Columbia University, New York, New York 10027, USA
[6]National Institute for Materials Science, 1-1 Namiki, Tsukuba 305-0044, Japan

(Received 29 December 2016; published 2 August 2017)

Coulomb interaction between two closely spaced parallel layers of conductors can generate the frictional drag effect by interlayer Coulomb scattering. Employing graphene double layers separated by few-layer hexagonal boron nitride, we investigate density tunable magneto- and Hall drag under strong magnetic fields. The observed large magnetodrag and Hall-drag signals can be related with Laudau level filling status of the drive and drag layers. We find that the sign and magnitude of the drag resistivity tensor can be quantitatively correlated to the variation of magnetoresistivity tensors in the drive and drag layers, confirming a theoretical formula for magnetodrag in the quantum Hall regime. The observed weak temperature dependence and $\sim B^2$ dependence of the magnetodrag are qualitatively explained by Coulomb scattering phase-space argument.

DOI: 10.1103/PhysRevLett.119.056802

Electronic double layers (EDL), consisting of two parallel conducting layers separated by a thin dielectric, provide a versatile platform to study interaction-driven phenomenon in two-dimensional (2D) systems. For example, the Bose-Einstein condensation of a magnetoexcitons in strongly interacting quantum Hall EDL has been discovered in GaAs EDL [1,2] and recently in graphene EDL [3,4]. The EDL can also be used to study resonance tunneling [5], proximity screening of disorder [6], and the penetration field [7].

Drag measurement in an EDL, i.e., applying the current $I_{\mathrm{drive}}$ in one of the layers (the "active" drive layer) and probing induced voltage $V_{\mathrm{drag}}$ in the other layer (the "passive" drag layer), has been a useful to tool to characterize the interlayer Coulomb interaction. In a weakly coupled regime at a finite temperature $T$, the drag resistance $R_{\mathrm{drag}} = V_{\mathrm{drag}}/I_{\mathrm{drive}}$ is typically dominated by the momentum transfer through interlayer electron-electron ($e$-$e$) scattering. This frictional drag effect has been studied in both semiconductor [8–10] and graphene EDLs [11,12]. In general, under zero magnetic fields, the EDLs can be described by the Fermi liquid theory, and a semiclassical picture can explain the observed frictional drag effect [13]. In this regime, two important features emerge: (1) drag is negative (positive) when two layers have the same (opposite) type of carriers, owing to the current and momentum relation, and (2) drag resistance scales with temperature as $R_{\mathrm{drag}} \propto T^2$, reflecting the increasing scattering phase space as temperature increases (Coulomb scattering phase-space argument) [8,13]. Recent studies in graphene EDL suggest that new drag mechanisms, other than the above-mentioned momentum drag, also play important roles near the double charge neutrality point (DNP) [11,14–18].

In the presence of magnetic fields, the momentum transfer direction in the drag process is not aligned with the drive current direction, and thus, drag voltages can be decomposed into magnetodrag (longitudinal component) and Hall drag (transverse component). Moreover, under strong magnetic fields, quantized Landau levels (LLs) form in both layers, requiring consideration beyond the semiclassical description. Early experimental works in GaAs EDLs revealed that the sign of magnetodrag depends on the LL filling factor difference between the two layers [19,20], which was not expected in a simple semiclassical model. Extending prior theoretical work based on the linear response theory [21–24], von Oppen, Simon, and Stern (OSS) proposed a theoretical approach to frictional drag under strong magnetic fields [25]. According to OSS, the drag resistivity tensor $\hat{\rho}^{\mathrm{drag}}$ can be related to the density differential of the magnetoconductivity tensors $\hat{\sigma}$ in individual layers

$$\hat{\rho}^{\mathrm{drag}} \sim -\hat{\rho}^{p}\frac{d\hat{\sigma}^{p}}{dn^{p}}\frac{d\hat{\sigma}^{a}}{dn^{a}}\hat{\rho}^{a}. \tag{1}$$

Here, $\hat{\sigma}$ and $\hat{\rho} \equiv \begin{pmatrix} \rho_{xx} & \rho_{xy} \\ \rho_{yx} & \rho_{yy} \end{pmatrix}$ are the magnetoresistivity and conductivity tensors, respectively, $n$ is carrier density of each layer, and the superscripts drag, $a$, and $p$ stand for the drag, active (drive), and passive (drag) layers, respectively. The physical interpretation of this theory is that driving dc current on one layer creates asymmetry in the thermal density fluctuations in that layer. These density fluctuations

 

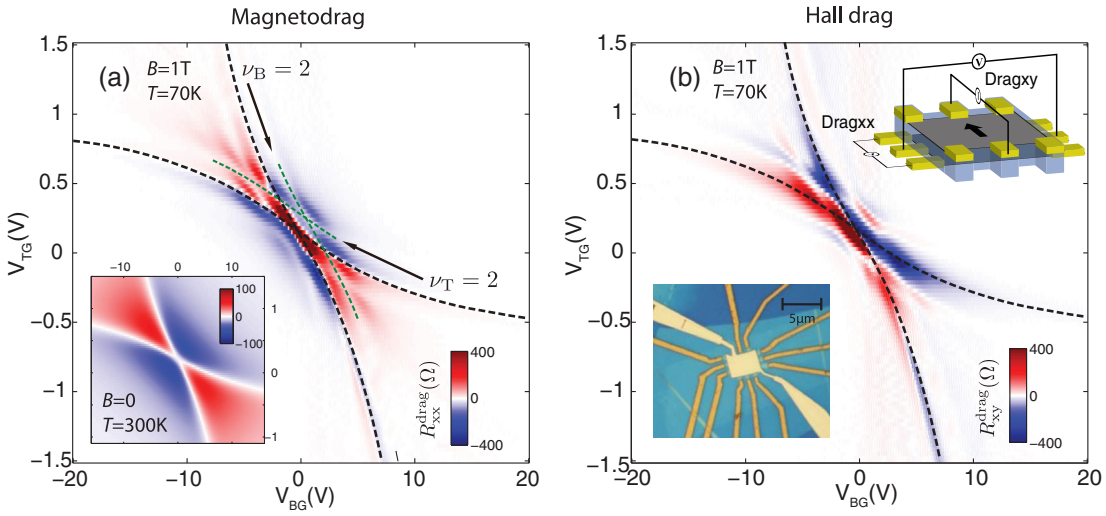


FIG. 1. (a) Magnetodrag resistance as a function of top gate ($V_{TG}$) and bottom gate voltages($V_{BG}$), measured under a magnetic field of 1 T and at a temperature of 70 K. Black and green dashed lines mark charge neutrality and $\nu = 2$ of the individual layers, respectively. The lower inset shows the drag resistance at zero magnetic field and a higher temperature of 300 K. (b) Hall-drag resistance under the same condition as (a). The upper insert shows the measurement schematics of the experiment. The lower inset shows an optical microscope image of the device used in this experiment.

are transferred to the drag layer through Coulomb interaction. Then, the induced density fluctuations in the drag layer are rectified to a dc voltage. This formula enables negative magnetodrag when the derivative of the conductivity tensor meets the right condition. It also predicts that Hall drag could have the same magnitude as the magnetodrag.

Graphene double-layer devices provide an excellent material platform to investigate the magnetodrag in the quantum limit, owing to a wide range of gate tunability of individual layers, large LL separation, and small interlayer distance. In this Letter, we present the experimental investigation of frictional magneto- and Hall drag in high-mobility graphene double layers. The observed drag can be quantitatively related to the modulation of the measured conductivity tensors in individual layers, confirming the OSS theory. Magnetic field and temperature dependence of the drag effect further reveal the nature of the Coulomb interaction between quantized LLs of the EDL systems.

The devices used in this experiment consist of two monolayer graphenes separated by a thin hexagonal boron nitride ($h$-BN) spacer ~4 nm, encapsulated by two thicker BN layers (~20 nm). The heterostructure is made using the dry transfer method [26], and edge contacts are fabricated on individual graphene layers [3,4]. The low-temperature (1.5 K) mobility of the bottom layer is ~50 $m^2/V\,s$, and the top layer shows a slightly lower mobility of ~20 $m^2/V\,s$. The high mobility we achieved in this device allows us to observe quantum Hall effect (QHE) at magnetic field $B$ as low as 0.2 T in both layers.

The drag measurements are performed by applying a small drive current $I_{drive} \sim 100$ nA to the (active) drive layer and by measuring the drag voltages in the (passive) drag layer. The low-frequency lock-in measurements (17.7 Hz) essentially probe the dc drag response. To eliminate spurious signals originating from interlayer bias gating effect [27], interlayer balancing is implemented in the drive layer [28]. The Onsager reciprocity and linear response of the drag signal to $I_{drive}$ are confirmed in our experiment. Interlayer tunneling resistance is found to be larger than the GΩ range. The magnetodrag resistance $R_{xx}^{drag}$ and Hall-drag resistance $R_{xy}^{drag}$ are obtained from the measured voltages across the passive (drag) layer. The drag data presented in this Letter are taken under both positive and negative magnetic fields and symmetrized (antisymmetrized) for $R_{xx}^{drag}$ ($R_{xy}^{drag}$) to remove mixing. Voltages applied to the back gate ($V_{BG}$) and the top gate ($V_{TG}$) control the carrier density of the drive layer (top) $n_T$ and the drag (bottom) layer $n_B$.

Figure 1 shows $R_{xx}^{drag}$ and $R_{xy}^{drag}$ as functions of $V_{BG}$ and $V_{TG}$, measured at $T = 70$ K, and a relatively low magnetic field $B = 1$ T. The two black dashed lines crossing each other correspond to $\nu_T = 0$ or $\nu_B = 0$, the charge neutrality point (CNP) of each layer. The top (bottom) layer carrier density is mainly tuned by $V_{TG}$ ($V_{BG}$). These CNP lines divide the ($V_{TG}$-$V_{BG}$) plane into four regions, $e$-$e$ (top right), $h$-$h$ (bottom left), $e$-$h$ (bottom right), and $h$-$e$ (top left). For magneto drag [Fig. 1(a)], the sign of $R_{xx}^{drag}$ follows the sign of drag at $B = 0$ [Fig. 1(a), inset]; i.e., the $e$-$e$ and $h$-$h$ regions exhibit a negative drag signal, while the $e$-$h$ and $h$-$e$ regions exhibit a positive drag, where $R_{xx}^{drag} \approx 0$ along the CNP lines dividing these regions. We also note that there is additional modulation in each region, where some $R_{xx}^{drag} \approx 0$ lines run parallel with CNP lines (examples are marked by green dashed lines). Further inspection in connection with the magnetoresistance measurements of

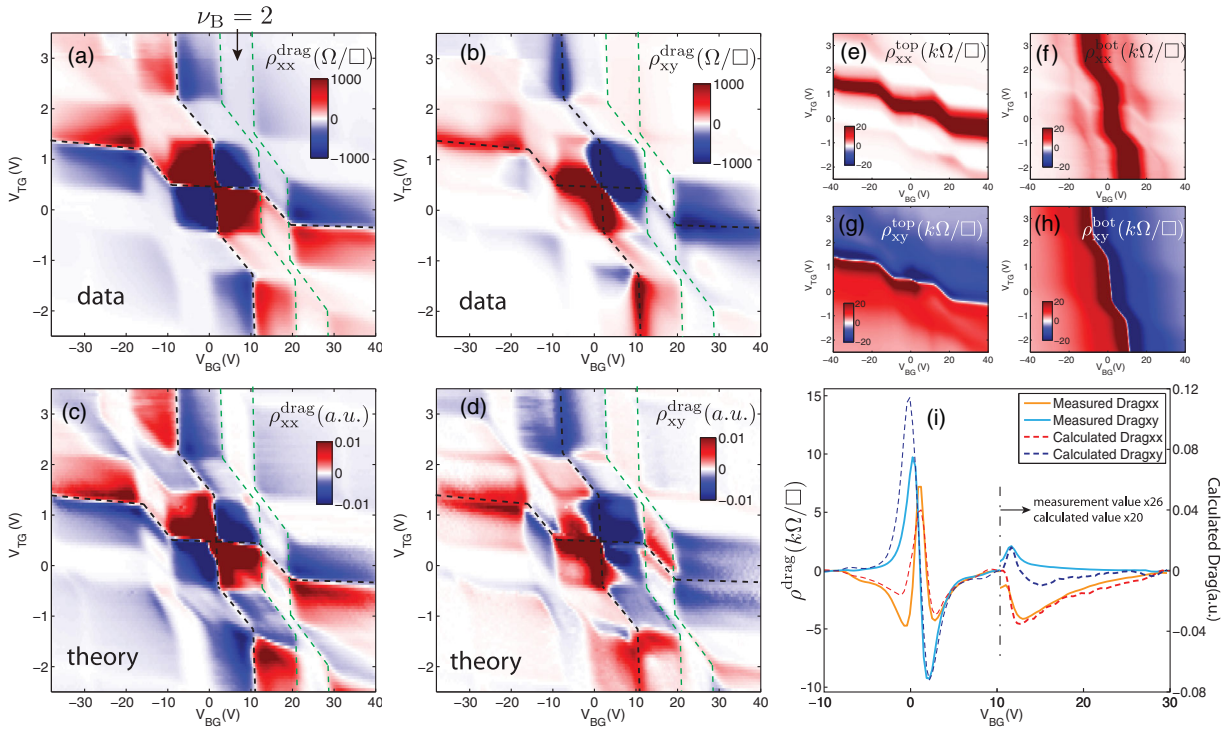


FIG. 2. (a),(b) Measured magneto- and Hall-drag resistivity at $T = 70$ K, $B = 13$ T. (c),(d) Calculated magneto- and Hall-drag resistivity using Eq. (1). The calculation is in arbitrary units (a.u.) due to the undetermined prefactor. The black dashed lines in (a)–(d) are charge neutrality lines of top and bottom layers. And the green outlined regions mark the $\nu_{top} = 2$ incompressible strip. (e),(f) Magnetoresistivity of top and bottom layers at $T = 70$ K, $B = 13$ T. (g),(h) Hall resistivity of top and bottom layers under the same condition. (i) Line cut of measured and calculated magneto- and Hall drag along the equal-density line ($n_T = n_B$). The dashed vertical line around $V_{BG} \approx 10$ V separates the first LL ($N = 1$) region (right) from the zeroth LL ($N = 0$) region (left). In the first LL region, measured drag is multiplied by a factor 26 for clarity, while the calculation is multiplied by a factor 20 in order to make a good comparison to the measured values.

each layer (which will be discussed later in detail) indicates that these lines are corresponding to $V_{TG}$, $V_{BG}$, where either the active or passive layers are in the quantum Hall (QH) states with integer LL filling fraction $\nu_T$ or $\nu_B$. The vanishing $R_{xx}^{drag}$ signal in these QH regions thus suggests that the drag becomes inefficient as the bulk of either layer becomes incompressible. The incompressible bulk results in zero density of the state for interlayer Coulomb scattering. This observation is more pronounced at higher magnetic fields where stronger QHE appears with a wide range of incompressible regions in the $V_{TG}$-$V_{BG}$ plane. Figure 2(a) shows $\rho_{xx}^{drag}(V_{TG}, V_{BG})$, measured at $B = 13$ T, where the well-developed zigzag-shaped incompressible stripes of QH states can be identified with zero drag (for example, the green dashed lines surround the $\nu_{bot} = 2$ incompressible strip where the drag vanishes). The zigzag shape of the CNP (black dashed lines) and other incompressible stripes originate from a difference of the screening effect inside and outside of LLs (nearly perfect screening inside LLs).

The corresponding Hall-drag $R_{xy}^{drag}$ measurements show similar vanishing signals in the incompressible regions in the $V_{TG}$-$V_{BG}$ plane, as shown in Fig. 1(b). We note $R_{xy}^{drag}$ exhibits a similar magnitude as $R_{xx}^{drag}$, confirming the prediction made by OSS in Eq. (1). However, unlike $R_{xx}^{drag}$, whose sign is determined by the sign of carriers, $R_{xy}^{drag}$ undergoes sign changes within each quadrant. Contrary to $R_{xx}^{drag}$, $R_{xy}^{drag}$ does not vanish along the CNP lines. At a higher magnetic field $B = 13$ T [Fig. 2(b)], the incompressible QHE regions exhibit well-developed regions of vanishing $\rho_{xy}^{drag}$, similar to $\rho_{xx}^{drag}$.

To compare density-dependent magneto- and Hall drag with Eq. (1), we obtain magnetotensors $\hat{\rho}$ and $\hat{\sigma}$ as a function of density. Experimentally, we measured the longitudinal ($R_{xx}$) and transverse ($R_{xy}$) components of magnetoresistance on each layer and then converted them to $\hat{\rho}$ and $\hat{\sigma}$, using simulated geometrical factors. Figures 2(e)–2(h) are measured $\rho_{xx}$ and $\rho_{xy}$, the two independent components of $\hat{\rho}$, of the top and bottom layers as a function of $V_{TG}$ and $V_{BG}$. These data were taken at the same condition as the drag experiment shown in Figs. 2(a)–2(b) and symmetrized (antisymmetrized) to remove mixing between $R_{xx}$ and $R_{xy}$. Under strong magnetic fields, the relation between the density and $V_T$ and $V_B$ can be complicated due to the screening effect in LLs. In general, the derivation of

conductivity, with respect to density $d\hat{\sigma}/dn$, thus includes derivation to both the top and bottom gates

$$\frac{d\hat{\sigma}}{dn} = \frac{d\hat{\sigma}}{dV_{\mathrm{BG}}}\frac{dV_{\mathrm{BG}}}{dn_B} + \frac{d\hat{\sigma}}{dV_{\mathrm{TG}}}\frac{dV_{\mathrm{TG}}}{dn_T}. \quad (2)$$

However, since $d\hat{\sigma}/dn$ is nonzero only in the compressible regions of $(V_T, V_B)$ where the gating effects decouple to each corresponding layer due to nearly perfect screening. In these regions, $n_T = C_{\mathrm{TG}}V_{\mathrm{TG}}/e$ and $n_B = C_{\mathrm{BG}}V_{\mathrm{BG}}/e$. Therefore, taking the derivative respect to densities is the same with respect to gate voltages times geometric capacitances.

Figures 2(c)–2(d) show the computed drag resistivity $\rho_{xx}^{\mathrm{drag}}$ and $\rho_{xy}^{\mathrm{drag}}$, obtained from $\hat{\rho}^{\mathrm{drag}}$ by applying experimentally obtained $\hat{\rho}^{a,p}$ to Eq. (1). $\hat{\sigma}^{a,p}$ were obtained by numerically inverting the $\hat{\rho}^{a,p}$ tensor. Comparing these calculated results with the measured drag resistivity shown in Figs. 2(a)–2(b), we find that theory provides a reasonable match to experiment by capturing key features of the sign and magnitude of the observed drag. To be specific, for $\rho_{xx}^{\mathrm{drag}}$, the calculation successfully captured that the sign of drag is governed by carrier types and does not change cross LLs for graphene EDL specifically. For $\rho_{xy}^{\mathrm{drag}}$, the complicated changes of Hall-drag signs are also revealed by the calculation. We note that while the calculated drag exhibits excellent agreement with the data in the compressible regime, the agreement between experiment and calculation is worse in the incompressible strips, especially for $\rho_{xy}^{\mathrm{drag}}$. Specifically, the measured drag signals vanish as expected, while the calculated ones do not. This is due to the imperfect measurement geometry [29] for $\rho_{xx}^{\mathrm{top}}$ and $\rho_{xy}^{\mathrm{bot}}$, which leads to a nonperfect QHE [as can be seen in Figs. 2(f) and 2(g)]. The nonperfect quantization results in finite $d\hat{\sigma}/dn$, which leads to nonzero calculated drag.

While comparing the absolute magnitude of experimental drags to theoretical expectation is not possible due to the undetermined prefactor in Eq. (1), we can still make a relative comparison of the magnitude of different components of the drag resistivity tensor. Figure 2(i) shows an example of such a comparison along the equal-density line ($n_T = n_B$). Note that the prefactor in Eq. (1) could be a function of density, temperature, and field. We multiplied a common factor to Eq. (1) to make the calculated results comparable to experimental $\hat{\rho}^{\mathrm{drag}}$. Plotting the magnetodrag and Hall drag in the same scale, we found that the relative magnitude between measured $\rho_{xx}^{\mathrm{drag}}$ and $\rho_{xy}^{\mathrm{drag}}$ (solid curves) match well with the calculation (dashed curves), proving that Eq. (1) holds quantitatively. For the best matching, we also note that we multiplied different common factors for different LLs, whose ratio is ~1.3 for the $N = 0$ to $N = 1$ Landau level (separated around $V_{\mathrm{BG}} \approx 10$ V), indicating that the prefactor in Eq. (1) can be LL dependent but has a weak density dependence within a LL.

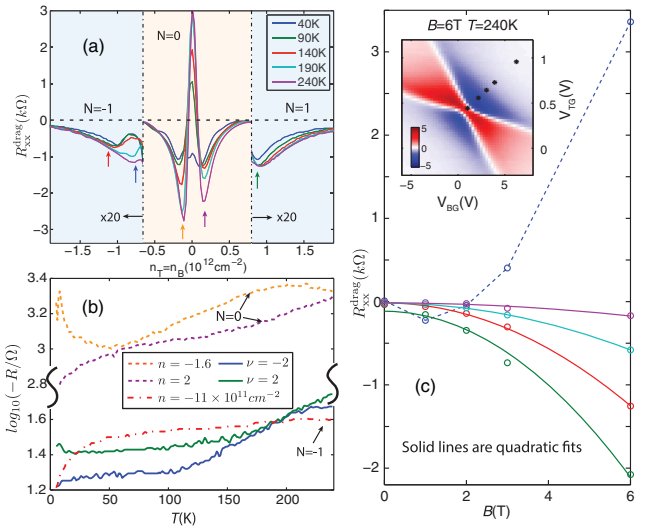


FIG. 3. (a) Magnetodrag along equal density line ($n_B = n_T$) as a function of densities at $B = 13$ T and different temperatures. The blue (yellow) shaded region marks $N = \pm 1$ ($N = 0$) LL. The drag signals are multiplied by a factor of 20 in the blue shaded regions for clarity. (b) Drag as a function of temperature at different density points. Solid lines represent the Landau gaps $\nu = \pm 2$. Dashed line represents partially filled LLs $n = -1.6$, $2 \times 10^{11}$ cm$^{-2}$, corresponding to $N = 0$ LL and $n = -11 \times 10^{11}$ cm$^{-2}$, corresponding to $N = -1$ LL. The density of each line in (b) is marked out in (a) by arrows with corresponding colors. (c) Magnetodrag as a function of the field at a temperature of 240 K at certain density points along equal density line (shown as * in the insert). Circles are experimental data, and solid curves are quadratic fits of the data.

Finally, we discuss the temperature and magnetic field dependence of drag signals. Unlike the zero-magnetic-field drag, which was found to be proportional to $T^2$, owing to the increasing scattering phase space in the Fermi liquid [11], $\rho_{xx}^{\mathrm{drag}}$ measured in the high-magnetic field regime exhibits a relatively weak temperature dependence. Figures 3(a) and 3(b) show the temperature- and density-dependent $\rho_{xx}^{\mathrm{drag}}$. We note that even for $N = 0$ LLs [orange shaded region in Fig. 3(a)], where we observed the most significant temperature dependence, the drag signals increase only by a factor of ~2 as temperature changes from 40 K to 240 K. In particular, when both layers are on the $N = \pm 1$ Landau level [red dashed line in Fig. 3(b)], there is almost no temperature dependence above ~40 K. The observed temperature-insensitive drag effect is presumably due to the fact that the thermal energy is much larger than the individual LL spreads, but much smaller than the LL spacing (the first cyclotron gap ~1500 K at $B = 13$ T). Under this condition, only one LL is partially occupied, while the LLs above or below are completed empty or full. And, as temperature is much larger than LL broadening, the entire partially filled LL is always accessible for Coulomb scattering. In this temperature regime (40 K to 240 K), temperature no longer controls

the scattering phase space, so drag no longer depends on temperature. At even lower temperatures ($T \sim 15$ K), a set of broken symmetry QHE emerges, and the agreement with the OSS theory persists [29]. We also note that there is a sign reversal of the magnetodrag at the double-charge neutrality point (i.e, $n_B = n_T = 0$), whose origin invites further investigation [29]. Interestingly, $\rho_{xx}^{\mathrm{drag}}$ exhibits a strong magnetic field dependence. Figure 3(c) shows $\rho_{xx}^{\mathrm{drag}}$ as a function of magnetic field at $T = 240$ K, where a $B^2$ dependence is observed across different densities. One possible explanation of the strong field dependence is that the scattering phase space is enlarged by the increase of the LL degeneracy at higher fields.

In conclusion, we measured magneto- and Hall drag in graphene double-layer heterostructures in the quantum Hall regime in the presence of strong thermal fluctuations. We observed strong drag signals, which vanish when either layer is in an incompressible quantum Hall state. The noted magneto- and Hall drag are well described by the variation of magnetotransport tensors in the drive and drag layers, confirming the material-independent theory proposed by OSS. As the OSS theory only accounts for drag caused by momentum transfer through Coulomb interaction, this also indicates that frictional momentum drag is the dominant mechanism for Coulomb drag in graphene EDL under a strong magnetic field.

We thank Felix von Oppen, Ady Stern, and Bertrand Halperin for helpful discussion. The major experimental work is supported by DOE (DE-SC0012260). P. K. acknowledges partial support from the Gordon and Betty Moore Foundation's EPiQS Initiative through Grant No. GBMF4543. K. W. and T. T. acknowledge support from the Elemental Strategy Initiative conducted by the MEXT, Japan. T. T. acknowledges support from a Grant-in-Aid for Scientific Research on Grant No. 262480621 and on Innovative Areas Nano Informatics (Grant No. 25106006) from JSPS.

*philipkim@g.harvard.edu

[1] J. Eisenstein, Annu. Rev. Condens. Matter Phys. **5**, 159 (2014).
[2] J. Eisenstein and A. MacDonald, Nature (London) **432**, 691 (2004).
[3] X. Liu, K. Watanabe, T. Taniguchi, B. I. Halperin, and P. Kim, arXiv:1608.03726.
[4] J. I. A. Li, T. Taniguchi, K. Watanabe, J. Hone, and C. R. Dean, arXiv:1608.05846.
[5] L. Britnell, R. V. Gorbachev, A. K. Geim, L. A. Ponomarenko, A. Mishchenko, M. T. Greenaway, T. M. Fromhold, K. S. Novoselov, and L. Eaves, Nat. Commun. **4**, 1794 (2013).
[6] L. A. Ponomarenko, A. K. Geim, A. A. Zhukov, R. Jalil, S. V. Morozov, K. S. Novoselov, I. V. Grigorieva, E. H. Hill, V. V. Cheianov, V. I. Fal'ko, K. Watanabe, T. Taniguchi, and R. V. Gorbachev, Nat. Phys. **7**, 958 (2011).
[7] K. Lee, B. Fallahazad, J. Xue, D. C. Dillen, K. Kim, T. Taniguchi, K. Watanabe, and E. Tutuc, Science **345**, 58 (2014).
[8] T. J. Gramila, J. P. Eisenstein, A. H. MacDonald, L. N. Pfeiffer, and K. W. West, Phys. Rev. Lett. **66**, 1216 (1991).
[9] P. M. Solomon, P. J. Price, D. J. Frank, and D. C. La Tulipe, Phys. Rev. Lett. **63**, 2508 (1989).
[10] U. Sivan, P. M. Solomon, and H. Shtrikman, Phys. Rev. Lett. **68**, 1196 (1992).
[11] R. V. Gorbachev, a. K. Geim, M. I. Katsnelson, K. S. Novoselov, T. Tudorovskiy, I. V. Grigorieva, a. H. MacDonald, S. V. Morozov, K. Watanabe, T. Taniguchi, and L. a. Ponomarenko, Nat. Phys. **8**, 896 (2012).
[12] S. Kim, I. Jo, J. Nah, Z. Yao, S. K. Banerjee, and E. Tutuc, Phys. Rev. B **83**, 161401 (2011).
[13] B. N. Narozhny and A. Levchenko, Rev. Mod. Phys. **88**, 025003 (2016).
[14] M. Titov, R. V. Gorbachev, B. N. Narozhny, T. Tudorovskiy, M. Schütt, P. M. Ostrovsky, I. V. Gornyi, A. D. Mirlin, M. I. Katsnelson, K. S. Novoselov, A. K. Geim, and L. A. Ponomarenko, Phys. Rev. Lett. **111**, 166601 (2013).
[15] K. Lee, J. Xue, D. C. Dillen, K. Watanabe, T. Taniguchi, and E. Tutuc, Phys. Rev. Lett. **117**, 046803 (2016).
[16] J. I. A. Li, T. Taniguchi, K. Watanabe, J. Hone, A. Levchenko, and C. R. Dean, Phys. Rev. Lett. **117**, 046802 (2016).
[17] J. C. W. Song, D. A. Abanin, and L. S. Levitov, Nano Lett. **13**, 3631 (2013).
[18] J. C. W. Song and L. S. Levitov, Phys. Rev. Lett. **111**, 126601 (2013).
[19] X. G. Feng, S. Zelakiewicz, H. Noh, T. J. Ragucci, T. J. Gramila, L. N. Pfeiffer, and K. W. West, Phys. Rev. Lett. **81**, 3219 (1998).
[20] J. G. S. Lok, S. Kraus, M. Pohlt, W. Dietsche, K. von Klitzing, W. Wegscheider, and M. Bichler, Phys. Rev. B **63**, 041305 (2001).
[21] A. Kamenev and Y. Oreg, Phys. Rev. B **52**, 7516 (1995).
[22] K. Flensberg, B. Hu, A. Jauho, and J. Kinaret, Phys. Rev. B **52**, 14761 (1995).
[23] B. N. Narozhny and I. L. Aleiner, Phys. Rev. Lett. **84**, 5383 (2000).
[24] B. N. Narozhny, I. L. Aleiner, and A. Stern, Phys. Rev. Lett. **86**, 3610 (2001).
[25] F. von Oppen, S. H. Simon, and A. Stern, Phys. Rev. Lett. **87**, 106803 (2001).
[26] L. Wang, I. Meric, P. Y. Huang, Q. Gao, Y. Gao, H. Tran, T. Taniguchi, K. Watanabe, L. M. Campos, D. a. Muller, J. Guo, P. Kim, J. Hone, K. L. Shepard, and C. R. Dean, Science **342**, 614 (2013).
[27] N. P. R. Hill, J. T. Nicholls, E. H. Linfield, M. Pepper, D. a. Ritchie, a. R. Hamilton, and G. a. C. Jones, J. Phys. Condens. Matter **8**, L557 (1996).
[28] M. Kellogg, Ph.D. thesis, California Institute of Technology, 2005.
[29] See Supplemental Material at http://link.aps.org/supplemental/10.1103/PhysRevLett.119.056802 for measurement details and supplementary data.